Journal of Solid Mechanics Vol. 5, No. 3 (2013) pp. 216-225

Numerical and Experimental Study on Ratcheting Behavior of Steel Cylindrical Shells with/without Cutout Under Cyclic Combined and Axial Loading

M. Shariati[1,*], K. Kolasangiani[2], H.R. Epakchi[2], H. Chavoshan[2]

[1] *Department of Mechanical University, Ferdowsi University of Mashhad, Mashhad, Iran*
[2]*Department of Mechanical University, Shahrood University of Technology, Shahrood, Iran*

Received 30 April 2013; accepted 20 June 2013

ABSTRACT

Ratcheting behavior of steel 304L cylindrical shell under cyclic combined and axial loading are investigated in this paper, numerically. Cylindrical shells were fixed oblique at angle of 20° and normal with respect to the longitudinal direction of the shell and subjected to force-controlled cycling with non-zero mean force, which causes the accumulation of plastic deformation or ratcheting behavior. Numerical analysis was carried out by ABAQUS software using nonlinear isotropic/kinematic hardening model. Numerical results compared to experimental data that was performed by an INSTRON 8802 servo hydraulic machine. Simulations show good agreement between numerical and experimental results. Also, the effect of length, angle of cylindrical shell and existence of cutout are studied with finite element method. Seen, the bending moment plays a strong role in increase of plastic deformation. It is observed that there is more plastic deformation for cylindrical shell under combined loading in comparison to cylindrical shell under uniaxial loading. Ratcheting behavior is sensitive to cutout and showed that creating the cutout increases the plastic deformation.

Keywords: Cylindrical shell; Numerical and experimental study; Cyclic combined and axial loading; Cutout

1 INTRODUCTION

CYLINDRICAL shells have numerous applications in aerospace industries as airplanes and missiles and also in pipelines, marine structures, power plants and nuclear plants. During their service life, the structures are subjected to cyclic loading of various types, where the stress state may exceed the elastic limit and degrade life of structural components [1, 2].

Ratcheting is a kind of special cyclic deformation behavior that occurs in materials and structures subjected to cyclic stressing with a non-zero mean stress, where the stresses are greater than the material's yield stress. Also, under cyclic loading with non-zero mean stress, some of the structures are equipped with cutout or crack. In this case, the crack growth occurred near the imperfection and the rate of ratcheting was increased [3]. So, ratcheting is one of the important factors that should be considered in the design of structural components and was extensively studied in last two decades. Most of experimental studies on cylindrical shells have been carried out by employing cyclic bending loadings [4-7]. Kang et al observed the uniaxial ratcheting behaviors of four metals (316L stainless steel, pure copper, pure aluminum and ordinary 20#carbon steel) with different crystal structures or values of fault

* Corresponding author. Tel.: +98 912 173 3750.
E-mail address: mshariati44@gmail.com (M. Shariati).

energy by the stress-controlled cyclic tests at room temperature [8]. Also, Kang et al have focused on the uniaxial and non-proportional multiaxial ratcheting behavior of SS304 stainless steel experimentally that the shapes of non-proportional loading paths were linear, circular, elliptical and rhombic in axial-torsional stress/strain space [9]. Mizuno et al have revealed some experimental results of uniaxial and multiaxial ratcheting for SS304 and 316 stainless steel and concluded some features of the ratcheting [10]. Shariati and hatami carried out experimental tests to study ratcheting behavior of SS304 cylindrical shells with/without cutout under axial loading. They observed that the rate of ratcheting became higher by using the higher force amplitude. Also, cutout caused ratcheting behavior in cylindrical shell extremely and increase of cutout radius showed more ratcheting strain than other specimens [11]. Shariati et al carried out experimental tests on the behavior of polyacetal or Polyoxymethylene (POM) under uniaxial cyclic loading. They showed that the ratcheting strain and strain rate ratcheting are sensitive to the applied stress amplitude and the mean stress [12]. Jiao et al performed an analysis on tubes. In this study, the effects of numbers of cycles with the mean stress and stress amplitude for specimens subjected to the constant internal pressure and cyclic axial load have been investigated [13]. Sun et al performed another numerical study on the behavior of stress-strain curve of cylindrical shells under combination of axial and torsional loads [14]. Dong et al simulated the hysteretic behaviors of channel and C-section cold-formed steel members (CFSMs) under cyclic axial loading with the finite element method (FEM) [15]. Shariati et al studied the behavior of hysteresis curve of cylindrical shells subjected to axisymmetric axial stress controlled and symmetric axial strain-controlled loadings in order to use the mechanical properties for numerical simulations [16].

In this paper, ratcheting behavior of steel cylindrical shell under combined and axial loading are studied using numerical simulation and compared to experimental results. It is observed that the plastic deformation for cylindrical shell under combined loading is larger than one under uniaxial loading.

2 NUMERICAL ANALYSIS USING THE FINITE ELEMET METHOD

The numerical simulations were carried out using the finite element software ABAQUS 6.10-1. This software between most ability, can be used for metals subjected to cyclic loading to analyze a kinematic hardening model with two parts, linear kinematic and nonlinear isotropic/kinematic hardening. The linear kinematic hardening model has a constant hardening modulus, and the nonlinear isotropic/kinematic hardening model has both nonlinear kinematic and nonlinear isotropic hardening components.

The evolution law of a linear kinematic hardening component describes the translation of the yield surface in stress space through the backstress, α. When temperature dependence is omitted, this evolution law is the linear Ziegler hardening law according to Eq. (1) [17].

$$\dot{\alpha}=C\frac{1}{\sigma^0}(\sigma_{ij}-\alpha_{ij})\dot{\bar{\varepsilon}}^{pl} \tag{1}$$

where $\dot{\bar{\varepsilon}}^{pl}$ is the equivalent plastic strain rate and *C* is the kinematic hardening modulus. In this model the equivalent stress defining the size of the yield surface, σ^0, remains constant, $\sigma^0=\sigma|_0$, where $\sigma|_0$ is the equivalent stress defining the size of the yield surface at zero plastic strain.

The evolution law of nonlinear isotropic/kinematic hardening model consists of two components: a nonlinear kinematic hardening component, which describes the translation of the yield surface in stress space through the backstress, α; and an isotropic hardening component, which describes the change of the equivalent stress defining the size of the yield surface, σ^0, as a function of plastic deformation.

The kinematic hardening component is defined to be an additive combination of a purely kinematic term (linear Ziegler hardening law) and a relaxation term (the recall term), which introduces the nonlinearity. In addition, several kinematic hardening components (backstresses) can be superposed, which may considerably improve results in some cases. When temperature and field variable dependencies are omitted, the hardening laws for each backstress are in Eq. (2) [17].

$$\dot{\alpha}=C\frac{1}{\sigma^0}(\sigma_{ij}-\alpha_{ij})\dot{\bar{\varepsilon}}^{pl}-\gamma\alpha_{ij}\dot{\bar{\varepsilon}}^{pl} \tag{2}$$

C and γ are material parameters that must be calibrated from cyclic test data. *C* is the initial kinematic hardening moduli, and γ determine the rate at which the kinematic hardening modulus decreases with increasing plastic deformation. The isotropic hardening behavior of the model defines the evolution of the yield surface size, σ^0, as a function of the equivalent plastic strain, $\bar{\varepsilon}^{pl}$. This evolution can be introduced by specifying σ^0 directly as a function of $\bar{\varepsilon}^{pl}$ in tabular form by using the simple exponential law in Eq. (3) [17].

$$\sigma^0=\sigma|_0+Q_\infty(1-e^{-b\bar{\varepsilon}^{pl}}) \tag{3}$$

where Q_∞ and b are material parameters. Q_∞ is the maximum change in the size of the yield surface, and b defines the rate at which the size of the yield surface changes as plastic straining develops. When the equivalent stress defining the size of the yield surface remains constant ($\sigma^0=\sigma|_0$), the model reduces to a nonlinear kinematic hardening model. In this paper, numerical analysis is accounted by the nonlinear isotropic/kinematic hardening model, because this model provides more accurate predictions.

In numerical analysis, cylindrical shells are placed oblique at angle of 20° and normal with respect to the longitudinal direction of the shells. Two ends of the cylindrical shell are bound with rigid cylinder that is inserted 20mm at the both ends of the specimen as shown in Fig. 1. So the efficient length (Leff) could be obtained by 20 mm reduce in length at both ends of cylindrical shells in combined and uniaxial loading. Each rigid cylinder has a reference point. Reference point in the above rigid cylinder with boundary condition of displacement/rotation type is bound to every direction. i.e. (U1=U2=U3=UR1=UR2=UR3=0). The lower reference point is bound to every direction except U3. Moreover, a sinus wave is allocated to amplitude parameter for periodical loading. Reference point in the lower rigid cylinder is subjected to cyclic loading under force-controlled condition with mean force and force amplitude 30kN and would be assigned to CF3 parameter (Fig. 2). Diagram forces containing axial force, bending moment and shear force acting on section at different length of cylindrical shell under combined loading are shown in Fig. 2b. The shear force can be neglected, because the thickness of the shells is low.

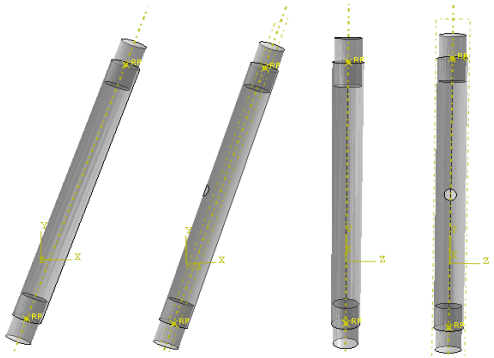

Fig. 1
Cylindrical shells simulated in numerical method under cyclic combined and axial loading.

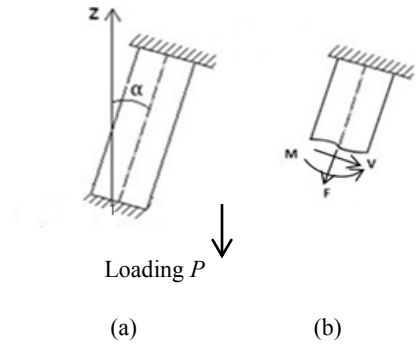

Fig. 2
(a) Schematic of combined loading on oblique cylindrical shell.
(b) Decomposition of applied combine load at different section of the shell (F=axial load, V=shear load and M=bending moment).

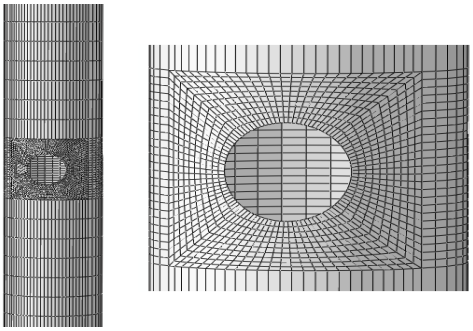

Fig. 3
A sample of FEM mesh.

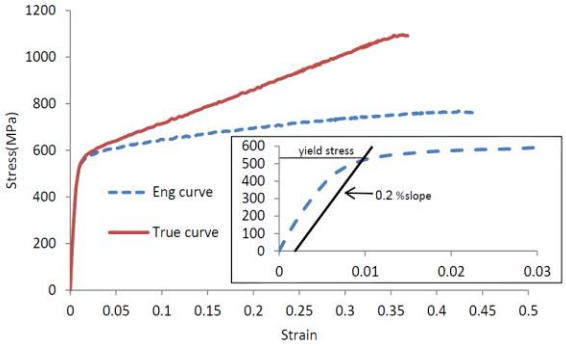

Fig. 4
Stress-strain curve of tension test for SS304L specimen.

Table 1
Geometrical and mechanical properties of the cylindrical shell

External Diameter	D=25.2mm
Thickness	t=1.4mm
length	L=240,340,440mm
Effective length	Leff=200,300,400mm
Modulus elasticity	E=202.495GPa
Yield stress	σ_y =513.01MPa
Ultimate stress	S_u =768.41MPa
Poisson's ratio	v=0.33

Element S8R5 was used in numerical simulation which is an eight node shell element with five degree of freedom in each node. For cylindrical shell with cutout, due to stress concentration around the cutout, size of the elements are smaller than another area. Part of a meshed specimen with cutout is shown in Fig. 3.

2.1 Geometry and mechanical properties of the shells

The material used in this work is SS304 stainless steel, which was acquired in the form of cylindrical shell by geometrical dimension, shown in Table 1. To determine the mechanical properties of SS304L, simple and standard tension test were performed according to ASTME A370-05 standard [18]. The obtained results are shown in Fig. 4.

The mechanical properties of specimens obtained from the experimental tests are shown in Table 1.

3 EXPERIMENTAL TESTS

The experimental device used in this study was a 250kN servo hydraulics INSTRON 8802 machine, as shown in Fig. 5. In standard tension test, a load cell with 25kN capacity and an extensometer were used to obtain mechanical properties of the specimens with higher accuracy.

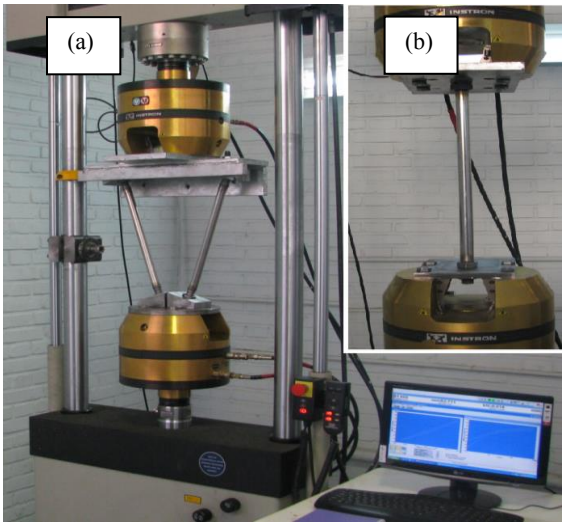

Fig. 5
INSTRON 8802 servo hydraulic machine, (a) combined loading, (b) axial loading.

Fixing ramp with an inclined plane of 20° was used in order to cylindrical shells were placed oblique on it and connecting to device jaw. Because specimens are thin, their two sided thread is not possible. So, threaded rods were inserted 20mm at the both ends of the specimens and welded to them. In order to avoid shear force and protect the device jaw from horizontal force during the oblique loading, two specimens were tested at the same time in the symmetrical position (Fig. 6). These kinds of fixtures are seen in article [19]. In uniaxial loading, threaded rods welded to the shell similar to combined loading and connected to device jaw without any fixtures which mimic the boundary conditions used in the finite element simulations in axial and combined loading.

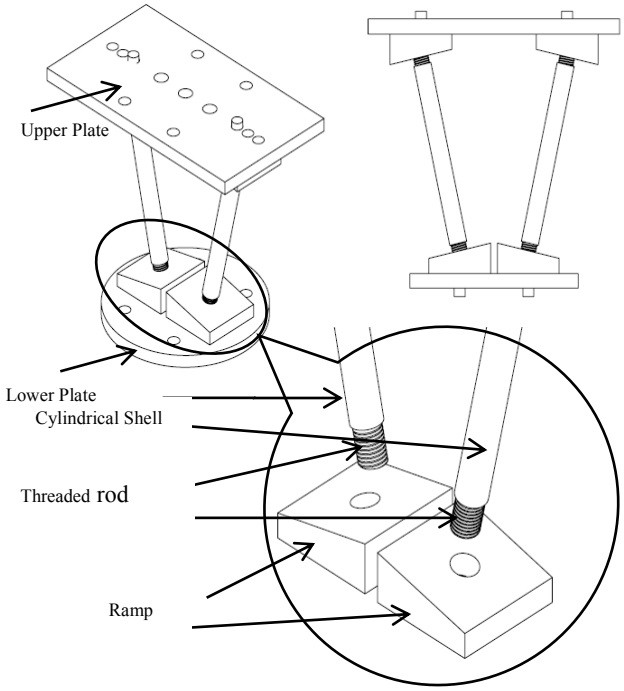

Fig. 6
Schematic of the cylindrical shells connected to the fixture using threaded rods and welding in combined loading.

4 CONFIRMATION OF NUMERICAL RESULTS WITH EXPERIMENTAL DATA

The results of experimental tests are compared with numerical finding in Figs. 7-10. To compare the plastic deformation in combined loading and uniaxial loading, in the present study, the ratcheting displacement will be defined as the maximum displacement each cycle. Generally, it is preferable to use dimensionless data for plotting the curves. Hence, so X_r will be defined as the ratio of ratcheting displacement to efficient length as illustrated in previous sections. It can be seen that ratcheting displacement is increased, whereas its rate is decreased continuously with increasing the cyclic number, in both numerical and experimental results. By comparing the experimental data with numerical results, we can see that the ABAQUS predicts appropriately in the initial cycles. But after a certain cycles, except for oblique cylindrical shell with cutout, numerical method give larger ratcheting displacement under the same loading condition. For oblique cylindrical shell with cutout in Fig. 10, due to existence of defects around the cutout in real specimen, ratcheting displacement is larger than one in numerical specimen. Because the materials are assumed to be ideal in the numerical analysis.

The largest bending moment was occurred at the ends of the shells and caused bending in the critical location at the ends of the shells that can be seen in experimental observations, as shown in Fig. 11.

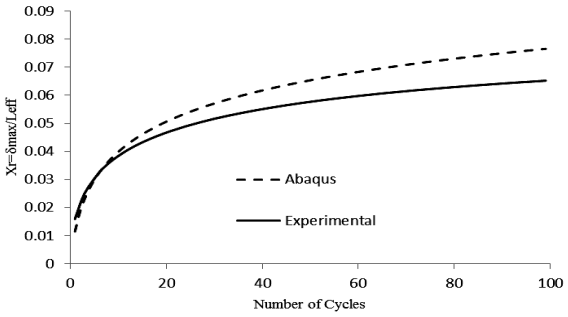

Fig. 7
Comparison of experimental and numerical ratcheting displacement for cylindrical shell with 440mm length under cyclic combined loading.

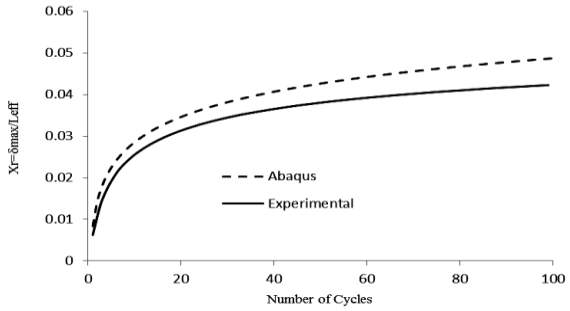

Fig. 8
Comparison of experimental and numerical ratcheting displacement for cylindrical shell with 240mm length under cyclic combined loading.

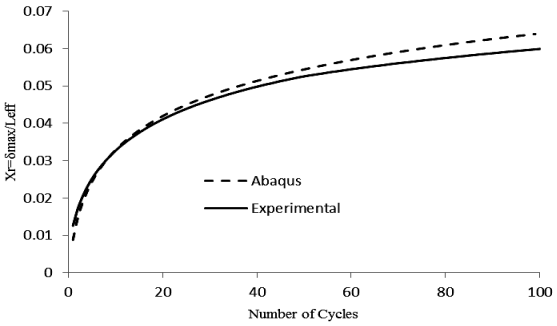

Fig. 9
Comparison of experimental and numerical ratcheting displacement for cylindrical shell with 440mm length under cyclic axial loading.

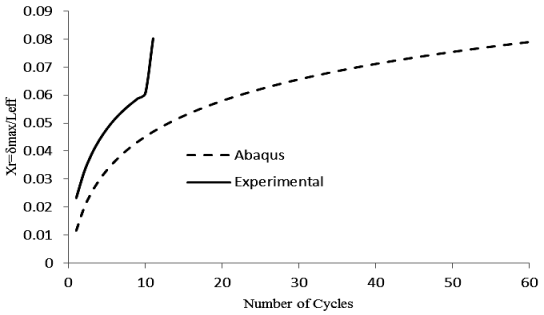

Fig. 10
Comparison of experimental and numerical ratcheting displacement for cylindrical shell with 440mm length with cutout under cyclic combined loading.

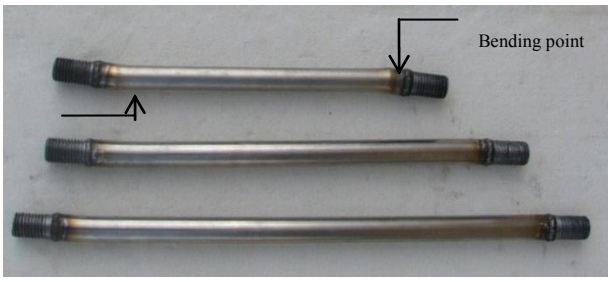

Fig. 11
Bending points at the ends of some cylindrical shells under combined loading after test.

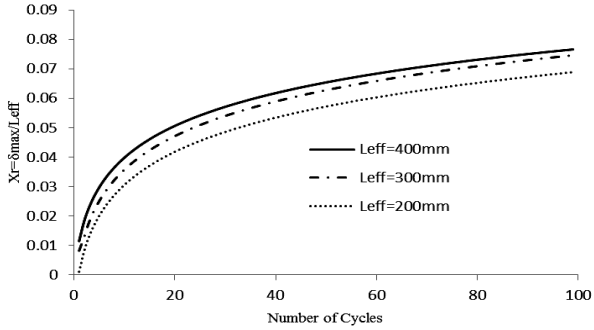

Fig. 12
Ratcheting displacement for different length of cylindrical shell under combined loading in numerical analysis.

5 RESULTS OF NUMERICAL ANALYSIS

5.1 Effect of shell length on ratcheting behavior of cylindrical shell under combined loading

In this section, cylindrical shells with 240mm, 340mm and 440mm length subjected to combined loading under the same loading condition. Fig. 12 shows ratcheting displacement versus number of cycles. It is observed that ratcheting displacement is higher for cylindrical shell with larger length, because the bending moment increases at different section of cylindrical shell with larger length.

5.2 Effect of shell angle on ratcheting behavior of cylindrical shell

Figs. 13-15 show the effect of shell angle on ratcheting behavior for cylindrical shell with 240mm, 340mm and 440mm length, respectively. It can be seen that ratcheting displacement for oblique cylindrical shell at angle of 20° under combined loading is larger than those under uniaxial loading. This kind of behavior is derived from existence of bending moment at different section of oblique cylindrical shell. So, superposition of bending moment and axial load for cylindrical shell under combined loading caused more plastic deformation compared to cylindrical shell under uniaxial loading. Also, for several cycles in the beginning of loading, the ratcheting displacement rate of shell

under combined loading is higher than one under uniaxial loading. Finally, ratcheting displacement rate of both types of loading becomes equal.

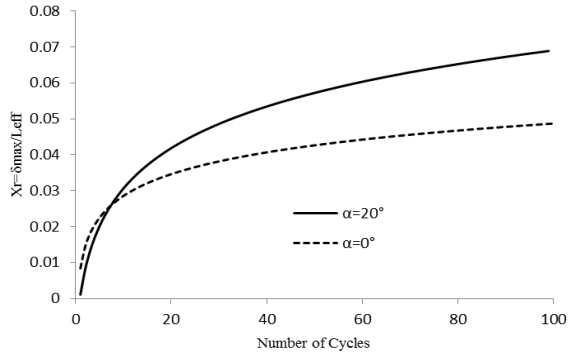

Fig. 13
Ratcheting displacement for two angles of cylindrical shell with 240mm length in numerical analysis.

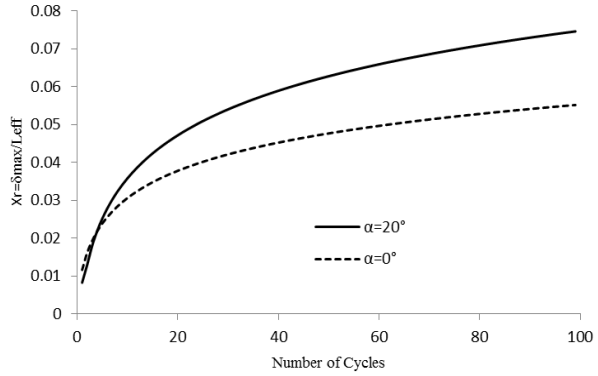

Fig. 14
Ratcheting displacement for two angles of cylindrical shell with 340mm length in numerical analysis.

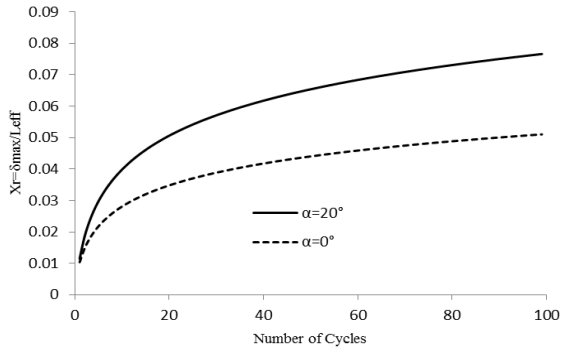

Fig. 15
Ratcheting displacement for two angles of cylindrical shell with 440mm length in numerical analysis.

5.3 Effect of cutout on ratcheting behavior of cylindrical shell

In order to analyze the effect of cutout on ratcheting behavior of cylindrical shell under combined and axial loading, a circular cutout with radius of 5mm was created in mid-height position of them and loaded in opening direction of cutout as shown in Fig. 1. According to Figs. 16-18, ratcheting displacement increases for cylindrical shell with cutout. Because existence of stress concentration around the cutout caused the plastic deformation increased in this area. Fig. 19 shows the von mises contour for oblique cylindrical shell with 440mm length under combined loading after 5 cycles. It can be seen that the regions around the cutout experience maximum stress and yield sooner than another area. Also, in the specimen with a cutout in mid-height position stress contour is totally symmetrical. The left side of the shell except around the cutout tolerates less stress because of the presence of the cutout.

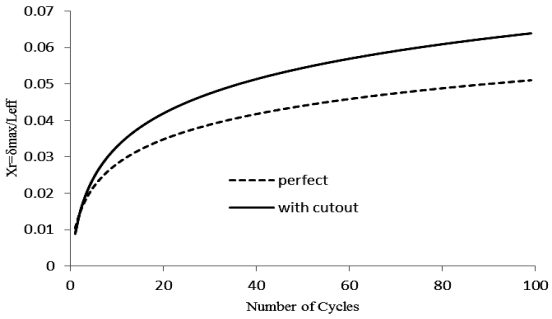

Fig. 16
Ratcheting displacement of cylindrical shells with/without cutout under axial loading with 440mm length in numerical analysis.

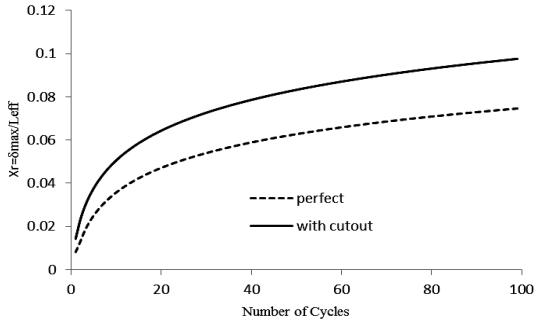

Fig. 17
Ratcheting displacement of cylindrical shells with/without cutout under combined loading with 340mm length in numerical analysis.

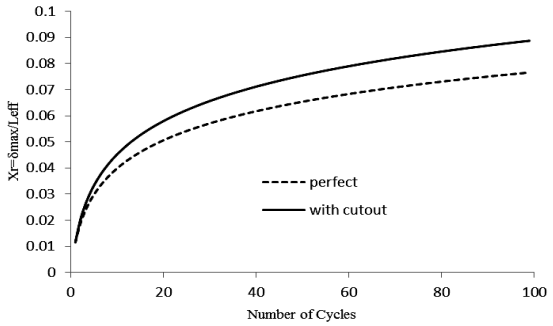

Fig. 18
Ratcheting displacement of cylindrical shells with/without cutout under combined loading with 440mm length in numerical analysis.

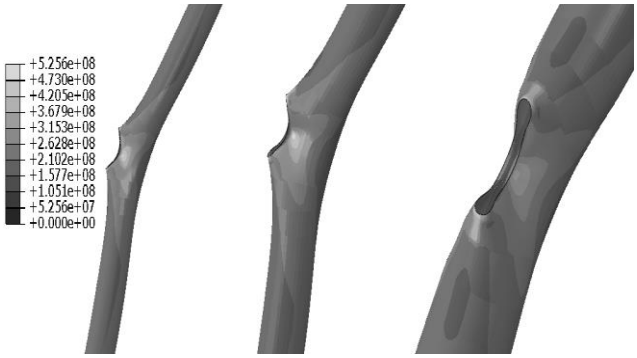

Fig. 19
Von mises stress contour for cylindrical shell under combined loading with 440mm length after 5 cycles.

6 CONCLUSIONS

In this research, the ratcheting behavior of cylindrical shells under combined and axial loading have been studied using numerical methodology and compared to experimental results. Based on the analysis of the results, the following conclusions were obtained:

1. Numerical simulation using nonlinear isotropic/kinematic hardening model predicts ratcheting behavior of cylindrical shell compared to experimental results.
2. The ratcheting displacement of cylindrical shell with cutout under combined loading is larger in numerical analysis than in experimental results due to existence of defect around the cutout in real specimen, which increases the ratcheting displacement in experimental test.
3. The largest bending moment was created at the ends of the shells under combined loading and caused the bending occurred in these points, considerably.
4. Due to existence of large bending moment at different section of oblique cylindrical shell with larger length, the ratcheting displacement is high as compared to oblique cylindrical shell with lower length.
5. The ratcheting displacement for cylindrical shell under combined loading is larger than one under uniaxial loading, because the bending moment cooperates with the axial load to increase the ratcheting displacement for cylindrical shell under combined loading.
6. Ratcheting displacement and its rate is higher for specimen with cutout compared to perfect specimen because stress concentration increases around the cutout and caused more plastic deformation.
7. In the specimen with a cutout in mid-height position stress contour is totally symmetrical and the side of the shell with cutout except around the cutout tolerates less stress compared to another side without cutout.

REFERENCES

[1] Ozgen U.C., 2008, Kinematic hardening rules for modeling uniaxial and multiaxial ratcheting, *Material & Design* **29**: 1575-1581.

[2] Isobe N., Sukekawa M., Nakayama Y., Date S., Ohtani T., Takahashi Y., Kasahara N., Shibamoto H., Nagashima H., Inoue K., 2008, Clarification of strain limits considering the ratcheting fatigue strength of 316FR steel, *Nuclear Engineering and Design* **238**: 347-352.

[3] Sih G.C., 1991, *Mechanics of Fracture Initiation and Propagation*, Kluwer Academic Publisher, Boston.

[4] Chang K.H., Pan W.F., Lee K.L., 2008, Mean moment effect of thin-walled tubes under cyclic bending, *Structural Engineering and Mechanics* **28**(5): 495-514.

[5] Rahman S.M., Hassan T., Corona E., 2008, Evaluation of cyclic plasticity models in ratcheting simulation of straight pipes under cyclic bending and steady internal pressure, *International Journal of Plasticity* **24**: 1756-1791.

[6] Chang K.H., Pan W.F., 2009, Buckling life estimation of circular tubes under cyclic bending, *International Journal of Solids and Structures* **46**: 254-270.

[7] Zakavi S.J., Zehsaz M., Eslami M.R., 2010, The ratcheting behavior of pressurized plain pipework subjected to cyclic bending moment with the combined hardening model, *Nuclear Engineering and Design* **240**: 726-737.

[8] Kang G., Liu Y., Dong Y., Gao Q., 2011, Uniaxial ratcheting behaviors of metals with different crystal structures or values of fault energy: macroscopic experiments, *Journal of Material Science and Technology* **27**(5): 453-459.

[9] Kang G.Z., Gao Q., Yang X.J., 2004, Uniaxial and non-proportionally multiaxial ratcheting of SS304 stainless steel at room temperature: experiments and simulations, *International Journal of Non-linear Mechanics* **39**: 843–857.

[10] Mizuno M., Mima Y., Abdel-Karim M., Ohno N., 2000, Uniaxial ratcheting of 316FR steel at room temperature, *Journal of Engineering Materials and Technology* **122**(1): 29–34.

[11] Shariati M., Hatami H., 2012, Experimental study of SS304L cylindrical shell with/ without cutout under cyclic axial loading, *Theoretical and Applied Fracture Mechanics* **58**: 35-43.

[12] Shariati M., Hatami H., Yarahmadi H., Eipakchi H.R., 2012, An experimental study on the ratcheting and fatigue behavior of polyacetal under uniaxial cyclic loading, *Materials and Design* **34**: 302–312.

[13] Jiao R., Kyriakides S., 2009, Ratcheting , wrinkling and collapse of tubes under axial cycling, *International Journal of Solids and Structures* **46**: 2856-2870.

[14] Sun G.Q., Shang D.G, 2010, Prediction of fatigue lifetime under multiaxial cyclic loading using finite element analysis, *Materials and Design* **31**(1): 126-133.

[15] Dong J., Wang S., Lu X., 2006, Simulations of the hysteretic behavior of thin-wall cold-formed steel members under cyclic uniaxial loading, *Structural Engineering and Mechanics* **24**(3): 323-337.

[16] Shariati M., Hatami H., Torabi H., Epakchi H.R., 2012, Experimental and numerical investigations on the ratcheting characteristics of cylindrical shell under cyclic axial loading, *Structural Engineering and Mechanics* **44**(6): 753-762.

[17] ABAQUS 6.10.1 PR11 user's manual.

[18] ASTM A370-05, Standard test methods and definitions for mechanical testing of steel products.

[19] Li Z., Yu J., Guo L., 2012, Deformation and energy absorption of aluminum foam-filled tubes subjected to oblique loading, *International Journal of Mechanical Science* **54**: 48-56.